

## Room-Temperature, Low-Barrier Boron Doping of Graphene

Lida Pan,<sup>†,‡</sup> Yande Que,<sup>‡</sup> Hui Chen,<sup>‡</sup> Dongfei Wang,<sup>‡</sup> Jun Li,<sup>‡</sup> Chengmin Shen,<sup>‡</sup> Wende Xiao,<sup>‡</sup> Shixuan Du,<sup>\*,‡</sup> Hongjun Gao,<sup>‡</sup> and Sokrates T. Pantelides<sup>\*,†,§,||</sup>

<sup>†</sup>Department of Physics and Astronomy, Vanderbilt University, Nashville, Tennessee 37235, United States

<sup>‡</sup>Institute of Physics, Chinese Academy of Sciences, Beijing 100190, P. R. China

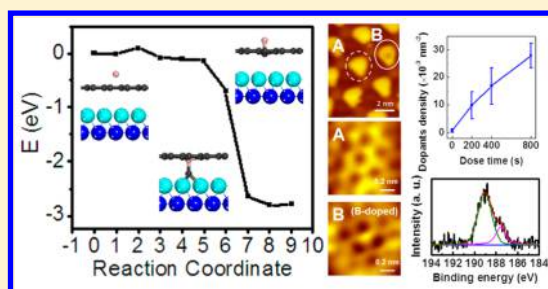
<sup>§</sup>Department of Electrical Engineering and Computer Science, Vanderbilt University, Nashville, Tennessee 37235, United States

<sup>||</sup>Materials Science and Technology Division, Oak Ridge National Laboratory, Oak Ridge, Tennessee 37831, United States

### Supporting Information

**ABSTRACT:** Doping graphene with boron has been difficult because of high reaction barriers. Here, we describe a low-energy reaction route derived from first-principles calculations and validated by experiments. We find that a boron atom on graphene on a ruthenium(0001) substrate can replace a carbon by pushing it through, with substrate attraction helping to reduce the barrier to only 0.1 eV, implying that the doping can take place at room temperature. High-quality graphene is grown on a Ru(0001) surface and exposed to B<sub>2</sub>H<sub>6</sub>. Scanning tunneling microscopy/spectroscopy and X-ray photoelectron spectroscopy confirmed that boron is indeed incorporated substitutionally without disturbing the graphene lattice.

**KEYWORDS:** boron-doped graphene, first-principles calculations, scanning tunneling microscopy, scanning tunneling spectroscopy



Monolayer graphene has generated great interest due to its unique properties and potential applications.<sup>1–10</sup> Its energy-band structure with the Fermi energy at a Dirac point leads to unusual electronic and magnetic properties, but a feature of many potential applications is the need to shift the Fermi energy away from the Dirac point, generating n-type or p-type graphene.<sup>11–15</sup> As in conventional three-dimensional semiconductors, one easily infers that such doping can be achieved by replacing C atoms with B atoms for p-type conduction and with N atoms for n-type conduction. The process for incorporating these elements in a graphene monolayer without concomitant disturbance of the lattice, however, has been difficult because of the strength of C–C bonds. In particular, calculations have shown that a B atom can push a C atom through free-standing monolayer graphene and replace it, but the activation barrier is high.<sup>16</sup> A common approach has been to use ion irradiation to create vacancies or divacancies, which can then easily accept substitutional impurities.<sup>17,18</sup> Although this process works, the quality of the graphene is degraded. Successful doping of graphene by adsorbates on the surface or at the edges of nanoribbons has been reported,<sup>19,20</sup> but such doping schemes are not as robust and controllable as substitutional doping by impurities.

In this paper, we report first-principles calculations that predict the possible doping of graphene by substitutional B by a room-temperature process and experimental confirmation of the process. The idea was motivated by the recent study on B atoms replacing C atoms in freestanding monolayer graphene<sup>16</sup> and Si penetrating through monolayer graphene.<sup>21–23</sup> We now report calculations showing that a B atom on top of monolayer

graphene on a ruthenium substrate simply pushes a C atom through and takes its place. The process is aided by the displaced C bonding with the Ru substrate, which reduces the energy barrier to effectively zero ( $\sim 0.1$  eV). The displaced C atom is initially attached to the B atom, but it migrates away with an activation energy of 0.8 eV. Thus, the process is predicted to work at room temperature. The process works for other substrates (Cu, Ir), also with very small barriers ( $\sim 0.2$  eV). A similar process using N has an energy barrier of 1.85 eV for a Ru substrate, which would require slightly elevated temperatures, but the same process next to substitutional B has a small barrier of 0.5 eV. Thus, the calculations predict the possibility of forming BN islands in monolayer graphene.

Experimental verification of the prediction of room-temperature doping by B was achieved. High-quality monolayer graphene was grown on Ru(0001) substrate and then exposed to B<sub>2</sub>H<sub>6</sub>, which can decompose to atomic boron at room temperature. As the exposure time increases, scanning tunneling microscopy (STM) topography shows more and more “dark spots” in the atop areas of the moiré pattern. Simultaneously, X-ray photoelectron spectroscopy (XPS) shows a new peak, indicating that C–B sp<sup>2</sup> bonds form. Therefore, we conclude that the dark spots are caused by boron atoms incorporated into the graphene sheet. High-resolution

Received: May 10, 2015

Revised: August 28, 2015

Published: September 8, 2015

STM images of the dark spots show explicitly that B atoms are incorporated substitutionally in the graphene lattice.

All calculations are performed within density functional theory (DFT) and the local density approximation (LDA),<sup>24</sup> using the Vienna ab initio simulation package (VASP).<sup>25,26</sup> The projector augmented wave (PAW) method<sup>27</sup> is employed. The electronic wave functions are expanded in plane waves with a kinetic energy cutoff of 400 eV. The k-points mesh used in the calculations is  $1 \times 1 \times 1$  owing to the large dimension of simulation supercell. The k-points mesh and other parameters were tested (see Supporting Information Figure S4). The structures are relaxed until residual forces are smaller than 0.01 eV/Å. A slab of Ru(0001) comprising two layers of Ru atoms was used, cleaved from crystalline Ru solid (lattice constants:  $a = 2.68$  Å,  $c = 4.22$  Å). A 8% compression of  $5 \times 5$  Ru(0001) substrate is used in order to fit the  $5 \times 5$  graphene supercell, and the slabs of Ru(0001) are kept fixed because of the calculation cost. A vacuum layer about 15 Å is used in the direction perpendicular to Ru(0001) substrate to avoid interactions between neighboring supercells.

First, we employ the climbing-image nudged elastic band (CI-NEB) method<sup>28</sup> to study the energy barrier of a single boron atom entering the graphene sheet by replacing one carbon atom. We choose a configuration of a single boron atom adsorbed on the bridge site of a pristine graphene sheet as the start of the doping process (Figure 1a). For the final

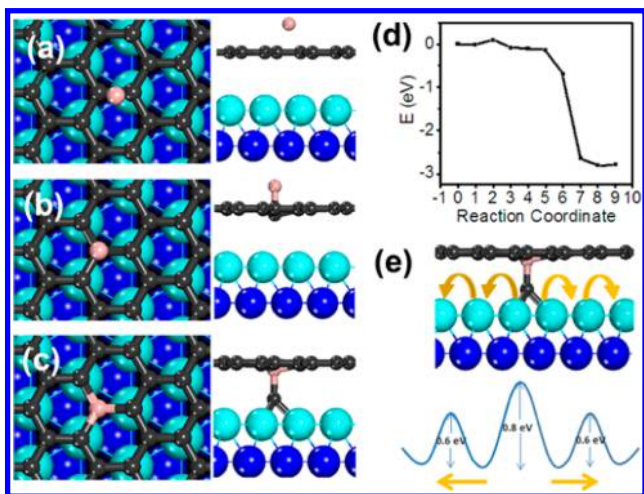


**Figure 1.** Schematic process of a boron atom being incorporated as a substitutional dopant in graphene. Light blue atoms are the top Ru surface layer; dark blue atoms are the second Ru layer. (a) Initial configuration (at the bridge site), (b) configuration with highest energy, where boron forms bonds with the carbon below, and (c) final configuration after doping is completed: the boron atom forms three bonds with neighboring carbon atoms and one carbon atom is pushed down to the substrate. (d) Energy barrier obtained from CI-NEB method. (e) Schematic process of a carbon atom diffusing between the interface of graphene and the Ru(0001) surface.

configuration after the doping, one carbon atom in graphene is replaced by boron, whereas the carbon atom is pushed down to the Ru(0001) surface just below the doping site (Figure 1c). The energy barrier along the whole path is shown in Figure 1d. The energy of the final state is lower by 3 eV compared with the initial state. Comparing with the results of ref 16, on the penetration of a B atom on free-standing monolayer graphene, it is clear that the decrease in the energy of the final state is mainly due to the interaction between the carbon atom and

substrate. The substrate effectively exerts an attractive force that drives the C atom down as the B takes the C atom's place.

The calculated energy barrier (Figure 1d) shows that there are three stages for the doping process. At the first stage (configurations 0 to 2), the energy increases slightly by 0.1 eV. It corresponds to the B atom beginning to merge into the graphene sheet while one C atom moves down slightly. At the maximum energy configuration, the distance between the B atom and the removed C atom is 1.7 Å, whereas the distance between the B atom and the substrate is 4.8 Å. Therefore, the increasing energy mainly comes from the interaction between the B atom and the graphene sheet. At the second stage (configurations 2 to 5), the energy begins decreasing but only by a small amount about 0.2 eV. In the third stage (configurations 5 to 8), the energy decreases drastically. At this stage, the C–C bonds are reformed as C–B bonds and the interaction between the displaced carbon atom and the substrate prevails. The energy barrier for the whole process is merely 0.1 eV, which suggests that the process can take place spontaneously at room temperature. To check how much the substrate affects the doping process, we take away the substrate and relax the doped structure. It shows that the displaced carbon atom goes back to the carbon sheet and boron-doped graphene is no longer a stable configuration. Therefore, the substrate plays an essential role for successful doping. More specifically, the process does not amount to simply replacing three C–C bonds with three B–C bonds, which is known to cost 1.3 eV in free-standing graphene.<sup>16</sup> Instead, three C–C bonds are gradually replaced by three C–B bonds, whereas the displaced C atom forms bonds with the B atom and three substrate Ru atoms, that is, it acquires tetrahedral bonding (see Figure 1c). It is the simultaneous formation of this B–C–Ru<sub>3</sub> bonded structure that reduces the barrier to essentially zero and leads to the large energy gain. After the displaced carbon moves away, though it looks like a boron atom has replaced a carbon atom in graphene, which is counterintuitive given the C–C and C–B bond strengths, the true final state of the system is a substitutional boron in the graphene plus an intercalated carbon atom. Such assistance by the substrate could also be provided by Cu(111) and Ir(111) substrates. Our calculations show that the energy barrier is  $\sim 0.2$  eV for these two substrates.

After the doping is complete, the next question is what happens to the C atom that was pushed below the graphene sheet. Figure 1d shows that the reverse process of the C atom going back to the graphene sheet has an energy barrier of about 3 eV. If the energy barrier of the C atom diffusing away is less than that, the carbon atom tends not to go back and the doping process is irreversible. Therefore, we examine the energy barrier for the intercalated C atom to make one step away from the substitutional B atom. This barrier is about 0.8 eV (Figure 1e), which also allows the process to occur at room temperature. The diffusion barrier further reduces to 0.6 eV when the C atom is farther away from the doping site. Therefore, the C is effectively free when it reaches the substrate, whereby it should be possible to obtain doped pristine graphene instead of some complex carbon–boron structures.

As noted earlier, the above results were obtained by compressing the Ru substrate by 8% in order to match a  $5 \times 5$  graphene supercell. Much larger and computationally costly supercells are needed to accommodate graphene on an uncompressed Ru substrate. The fact that we found that the activation barrier for the B doping process is essentially zero suggests that the error introduced by compressing the Ru

substrate is not likely to negate the conclusion that the barrier is in fact small enough for the process to occur at room temperature. We proceeded, therefore to test the theoretical prediction by performing experiments, which we describe next.

Samples were fabricated on Ru(0001) crystals in ultrahigh vacuum (UHV) LT-STM system. These Ru(0001) crystals were cleaned ultrasonically in high-purity acetone and ethanol to remove organic contaminations on the surface. Prior to the growth of graphene, the Ru(0001) surface was further cleaned by several cycles of ion sputtering using Ar<sup>+</sup> with energy of 1 keV and annealing at 1400 K in UHV chamber. Single-layer graphene was epitaxially grown on Ru(0001) via pyrolysis of ethylene (C<sub>2</sub>H<sub>4</sub>). The quality of the as-grown graphene was checked by STM. Boron-doped graphene was prepared by exposing the as-grown graphene/Ru to diborane (B<sub>2</sub>H<sub>6</sub>) at room temperature. STM images were acquired in constant-current mode, and all given voltage refer to the sample. Differential conductance (dI/dV) spectra and maps were acquired by using a lock-in technique with a 5 mV<sub>rms</sub> sinusoidal modulation at 973 Hz, which is superposed to the bias voltage V<sub>bias</sub>. All the measurements were carried out at ~4.2 K with electrochemically etched tungsten tips, which were calibrated against the surface states of the Au(111) surface prior to the spectroscopic measurements.

Figure 2a shows the clean graphene surface as imaged by STM. It reveals the characteristic moiré pattern, which has been

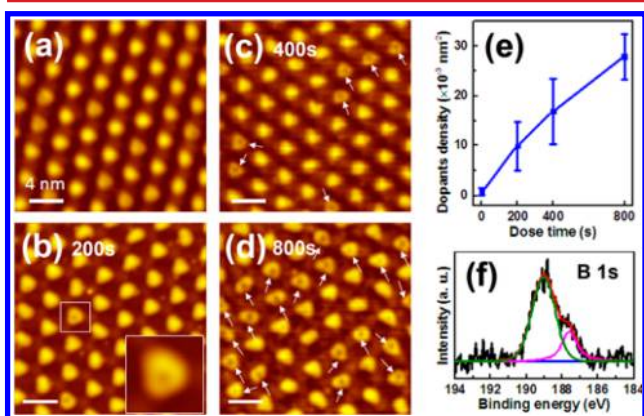


**Figure 2.** STM images and XPS spectra of boron-doped graphene on Ru(0001). (a) Moiré pattern of clean graphene on Ru(0001). (b)–(d) Graphene exposed to diborane at room temperature for 200, 400, and 800 s, respectively (tunneling gap: sample bias  $V_{\text{bias}} = -200$  mV, tunneling current  $I_{\text{set}} = 10$  pA). (e) B-dopant density in graphene/Ru vs dosing time. The dopant density was acquired by counting the number of B dopants in  $50 \times 50$  nm<sup>2</sup> (over two samples, 5 areas for each sample). (f) XPS spectra of B-doped graphene on Ru(0001).

ascribed to geometric and electronic effects.<sup>29–31</sup> We note that each unit cell of the moiré pattern includes three different regions: atop, fcc, and hcp regions. Figure 2b shows the graphene monolayer after it is exposed to diborane ( $1 \times 10^{-5}$  mbar) at room temperature for 200 s. In contrast to the clean graphene surface, a few dark spots located at the atop regions appear. Increased boron exposure time leads to an increasing density of such dark spots, as shown in Figure 2c,d. Similar features were found in multiple measurements, as illustrated in Supporting Information Figure S1. By counting the number of dark spots, we arrive at a concentration of such dark spots as a function of boron exposure, which is approximately propor-

tional to the dose time of boron, as shown in Figure 2e, leading us to associate these dark-spots with B dopants.

To confirm that the dark spots are caused by B dopants, we performed XPS for pristine and B-doped samples (Figure 2f). After exposure to B<sub>2</sub>H<sub>6</sub>, XPS shows two additional peaks at 187.6 and 189.1 eV in the XPS spectrum. The peak with lower binding energy (centered at 187.6 eV) is related to non-stoichiometric B<sub>x</sub>C<sub>y</sub>, and B-doped carbon nanoparticles.<sup>32,33</sup> The STM image for nanoparticles is shown in Supporting Information Figure S3. The peak with binding energy of 189.1 eV can be associated with sp<sup>2</sup> C–B bonds<sup>33,34</sup> present in graphene, indicating the formation of substitutional bonds. It is clear that sp<sup>2</sup> C–B bonds, that is, B doping, dominates.

In order to unveil the detailed structure of B dopants in the graphene lattice, we acquired atomically resolved STM images of B-doped graphene on Ru(0001). Figure 3a shows a

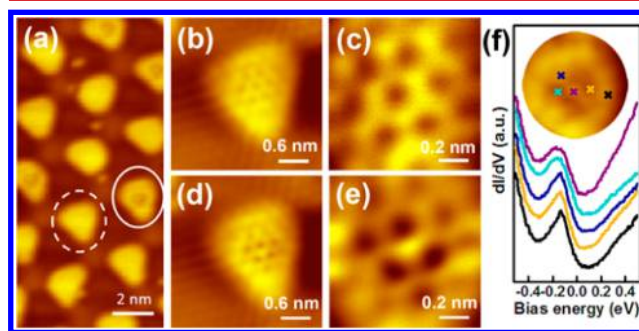


**Figure 3.** STM imaging of B dopants. (a) STM image of the most common doping form observed on B-doped graphene on Ru(0001) ( $V_{\text{bias}} = -120$  mV,  $I_{\text{set}} = 10$  pA); (b)–(e) Atomically resolved STM images of graphene/Ru(0001) around atop regions with and without B dopant showing honeycomb lattice of graphene, respectively (b,  $V_{\text{bias}} = -85$  mV; d,  $-200$  mV,  $I_{\text{set}} = 300$  pA; c,  $V_{\text{bias}} = -150$  mV,  $I_{\text{set}} = 310$  pA; e,  $V_{\text{bias}} = -200$  mV,  $I_{\text{set}} = 1$  nA). The B dopants in the lattice have an apparent out-of-plane height of ~0.2 Å. (f) dI/dV curves taken on a B atom (top) and on surrounding atoms near the B atom on B-doped graphene on Ru(0001), offset vertically for clarity (tunneling gap:  $V_{\text{bias}} = -200$  mV,  $I_{\text{set}} = 100$  pA). (Inset) positions where the spectra were taken.

representative STM topography of B-doped graphene. The dashed circle indicates an undoped atop region. Its close-up topography is shown in Figure 3b,c. The solid-line circle in Figure 3a indicates a doped atop region. Its close-up topography is shown in Figure 3d,e. Figure 3e reveals one bright spot connecting to three less-bright spots in the honeycomb lattice. We infer that the central bright spot is the B dopant, which is bonded to three carbon atoms. We note that boron atoms appear dark in the low-resolutions image, whereas they appear bright in the high-resolution image. This effect arises because a low-resolutions spot is an average of the bright boron spot and the surrounding three dark spots in the low-resolution image. The dark spots clearly overwhelm the central bright spot and the region appears dark. Figure 3c shows the honeycomb structure of the graphene lattice with C–C distance of  $1.64 \pm 0.12$  Å, indicating large tension strain<sup>35</sup> in the graphene lattice in these atop regions ( $1.42$  Å for that of free graphene), due to the strong interaction between graphene and the Ru substrate. The brighter B atoms in the high-resolution image are consistent with similar STM observation in B-doped graphene on a Cu substrate in ref 12. The low-resolution images are different in the two papers because of the

different substrates (different hybridization of  $\pi$ -bands in graphene with 3d bands in Ru or Cu substrate). We note that defects in graphene and adsorbates on graphene may also be introduced during the exposure to boron, which could result in change in STM topography. However, the intact honeycomb lattice shown in Figure 3d,e suggests the absence of such defects. Furthermore, adsorbates on graphene can also be excluded as the origin of the dark spots because adsorption of molecules or atoms on graphene would result in large protrusion in STM topography,<sup>36,37</sup> which is not in agreement with our high-resolution STM results. In addition, we also note that a few small bright spots were found in other two regions (fcc and hcp) besides the dopants in the atop regions after exposure to boron, as presented in Figures 2 and 3 as well as Supporting Information Figure S2b. These spots disappeared after annealing at 800 K (Supporting Information Figure S2c), indicating that they are not stable at high temperature, whereas boron dopants in the atop regions are stable even at higher temperature. Furthermore, the B dopant atom can be distinguished from the surrounding C atoms in the graphene lattice by detailed STS measurements on B-doped graphene samples. Figure 3f shows five differential conductance ( $dI/dV$ ) spectra on (the top violet curve) and around (the bottom four curves) a B dopant. All the curves show two most prominent features in the spectra: the depression near zero bias energy and the state around  $-140$  meV, which has been seen previously on monolayer graphene on Ru(0001).<sup>30,38</sup> The pronounced difference occurs above the Fermi energy ( $E_F$ ). For empty states above  $\sim 150$  meV, the intensity of  $dI/dV$  spectrum increases more sharply with energy on the B dopant atom than that on its surroundings.

The electronic nature of the graphene film is affected by the rippling and the presence of the B atoms. In Figure 4a, we show

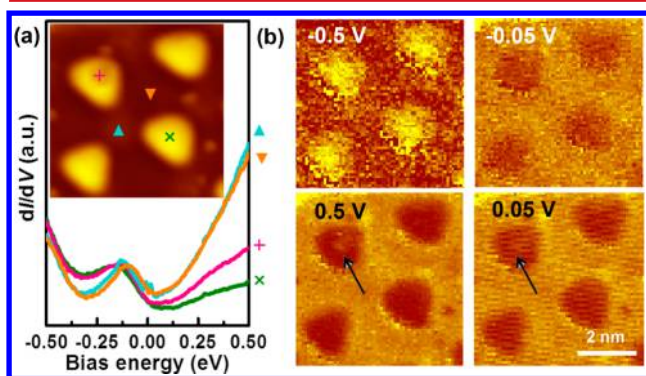


**Figure 4.** Spectroscopy and spectroscopic mapping around B dopants. (a)  $dI/dV$  spectra taken on the B atom and its surrounding area for B-doped graphene/Ru(0001). (Inset) positions where the spectra were taken; (b) STS maps taken in the vicinity of a single B dopant for B-doped graphene on Ru(0001) at different energies. (Tunneling gap:  $V_{\text{bias}} = -200$  mV,  $I_{\text{set}} = 100$  pA). The black arrows point to bright features at the center of the doped atop region (pink + symbol in (a)).

spectra on (denoted by pink plus symbol) and far away (areas within one unit cell of the moiré pattern) from a B dopant atom. Although the overall features of the spectra are almost the same, the spectra reveal the redistribution of the density of states (DOS) of graphene on Ru(0001) in the atop, fcc, hcp regions, indicating the corrugations in the STM topography are the results of electronic structures. In addition, the spectra show the enhancement of DOS above  $E_F$  on the B dopant, compared

to that on the corresponding position at the undoped atop region. To assess the amount of scattering introduced by the dopant, we performed  $dI/dV$  mapping in a  $6 \times 6$  nm<sup>2</sup> area containing a unit cell of moiré pattern with one graphitic B dopant. Figure 4b shows a subset of these maps, acquired at bias voltage from  $-0.5$  to  $0.5$  V. Although in the STM images the atop regions are brighter, they are darker in the STS maps at positive voltage. In Figure 4b, the black arrows point to extra intensity in one atop region, which is consistent with the STM image of the same region in Figure 4a, indicating the presence of boron.

Overall, the experimental evidence for substitutional boron doping can be summarized as follows. Both the STM images and STS maps show that a number of atop regions contain distinct features. In these features, at the atomic scale, a substitutional single atom in-plane in the graphene network is distinct from the others, whereas the network remains intact. The number of atop regions containing these distinct features correlates linearly with the boron dose, and XPS data shows the appearance of C–B  $sp^2$  bonds. We conclude, therefore that the distinct atoms at substitutional sites are boron atoms.

To date, much effort has been focused on nitrogen doping to fabricate n-type graphene. Thus, it is helpful to examine a similar doping mechanism applied to nitrogen doping. Calculations have found that the energy barrier of nitrogen is larger compared with that of boron. When the carbon atom starts being “kicked off”, the energy barrier undergoes an almost linear increase. After the highest point, the energy has a drastic dropping, which is caused by the bond forming between the kicked-off carbon atom and the substrate. The energy barrier for this process is about 1.85 eV. The energy decreases by 1.7 eV from the initial state to the final. The barrier of the carbon atom diffusing across the interface is about 0.8 eV. Although the doping process for nitrogen entails a higher energy barrier, it is found that if a boron atom is first introduced to the graphene sheet, followed by a nitrogen atom, the energy barrier to incorporate the N atom substitutionally next to the B atom is reduced to 0.5 eV. This result suggests that the N doping is enhanced when B dopant is present.

In summary, we used first-principles calculations to reveal a reaction path of a single boron atom replacing one carbon atom in graphene on a Ru(0001) substrate with an energy barrier of merely 0.1 eV. The substrate effectively exerts a driving force to pull the C atom down and the C atom then migrates away. We further demonstrated experimentally that the process works, that is, one can fabricate B-doped graphene at room temperature. We confirmed the presence of B dopants in the graphene lattice by performing XPS for a pristine and boron-doped samples. Furthermore, atomically resolved STM images and STS spectra and maps show that single boron dopants are incorporated into the monolayer graphene sheet.

## ■ ASSOCIATED CONTENT

### Supporting Information

The Supporting Information is available free of charge on the ACS Publications website at DOI: 10.1021/acs.nanolett.5b01839.

Additional information on STM images of boron dopants in other areas, the region dependence for boron doping, STM image for boron nanoparticles and calculation details. (PDF)

## AUTHOR INFORMATION

### Corresponding Authors

\*E-mail: [sxdu@iphy.ac.cn](mailto:sxdu@iphy.ac.cn) (S.D.).

\*E-mail: [pantelides@vanderbilt.edu](mailto:pantelides@vanderbilt.edu) (S.T.P.).

### Author Contributions

The manuscript was written through contributions of all authors. All authors have given approval to the final version of the manuscript. L.P. and Y.Q. contributed equally.

### Notes

The authors declare no competing financial interest.

## ACKNOWLEDGMENTS

This work was supported by grants from the National Science Foundation of China (51210003, 61390500, 51325204), National “973” projects of China (2013CBA01601, 2011CB921702), the Chinese Academy of Sciences, SSC, by the U.S. Department of Energy grant DE-FG02-09ER46554, and by the McMinn Endowment at Vanderbilt University.

## REFERENCES

- (1) Novoselov, K. S.; Geim, A. K.; Morozov, S. V.; Jiang, D.; Grigorieva, M. K. I.; Dubonos, S. V.; Firsov, A. A. *Nature* **2005**, *438*, 197–200.
- (2) Geim, A. K.; Novoselov, K. S. *Nat. Mater.* **2007**, *6*, 183–191.
- (3) Katsnelson, M.; Novoselov, K.; Geim, A. *Nat. Phys.* **2006**, *2*, 620–625.
- (4) Meyer, J. C.; Geim, A. K.; Katsnelson, M.; Novoselov, K.; Booth, T.; Roth, S. *Nature* **2007**, *446*, 60–63.
- (5) Neto, A. C.; Guinea, F.; Peres, N.; Novoselov, K. S.; Geim, A. K. *Rev. Mod. Phys.* **2009**, *81*, 109–162.
- (6) Novoselov, K. S.; Geim, A. K.; Morozov, S.; Jiang, D.; Zhang, Y.; Dubonos, S.; Grigorieva, I.; Firsov, A. *Science* **2004**, *306*, 666–669.
- (7) Novoselov, K. S.; Fal, V.; Colombo, L.; Gellert, P.; Schwab, M.; Kim, K. *Nature* **2012**, *490*, 192–200.
- (8) Schedin, F.; Geim, A.; Morozov, S.; Hill, E.; Blake, P.; Katsnelson, M.; Novoselov, K. *Nat. Mater.* **2007**, *6*, 652–655.
- (9) Xia, F.; Mueller, T.; Lin, Y.-m.; Valdes-Garcia, A.; Avouris, P. *Nat. Nanotechnol.* **2009**, *4*, 839–843.
- (10) Lin, Y. M.; Dimitrakopoulos, C.; Jenkins, K. A.; Farmer, D. B.; Chiu, H. Y.; Grill, A.; Avouris, P. *Science* **2010**, *327*, 662–662.
- (11) Gong, Y.; Shi, G.; Zhang, Z.; Zhou, W.; Jung, J.; Gao, W.; Ma, L.; Yang, Y.; Yang, S.; You, G. *Nat. Commun.* **2014**, *5*, 3193.
- (12) Zhao, L.; Levendorf, M.; Goncher, S.; Schiros, T.; Palova, L.; Zabet-Khosousi, A.; Rim, K. T.; Gutiérrez, C.; Nordlund, D.; Jaye, C. *Nano Lett.* **2013**, *13*, 4659–4665.
- (13) Zhao, L.; He, R.; Rim, K. T.; Schiros, T.; Kim, K. S.; Zhou, H.; Gutiérrez, C.; Chockalingam, S.; Arguello, C. J.; Pálová, L. *Science* **2011**, *333*, 999–1003.
- (14) Lu, Y. F.; Lo, S. T.; Lin, J. C.; Zhang, W.; Lu, J. Y.; Liu, F. H.; Tseng, C. M.; Lee, Y. H.; Liang, C. T.; Li, L. J. *ACS Nano* **2013**, *7*, 6522–6532.
- (15) Schiros, T.; Nordlund, D.; Pálová, L.; Prezzi, D.; Zhao, L.; Kim, K. S.; Wurstbauer, U.; Gutiérrez, C.; Delongchamp, D.; Jaye, C. *Nano Lett.* **2012**, *12*, 4025–4031.
- (16) Tsetseris, L.; Pantelides, S. T. *Carbon* **2014**, *67*, 58–63.
- (17) Guo, B.; Liu, Q.; Chen, E.; Zhu, H.; Fang, L.; Gong, J. R. *Nano Lett.* **2010**, *10*, 4975–4980.
- (18) Wang, H.; Wang, Q.; Cheng, Y.; Li, K.; Yao, Y.; Zhang, Q.; Dong, C.; Wang, P.; Schwingenschlög, U.; Yang, W. *Nano Lett.* **2011**, *12*, 141–144.
- (19) Wang, X.; Li, X.; Zhang, L.; Yoon, Y.; Weber, P. K.; Wang, H.; Guo, J.; Dai, H. *Science* **2009**, *324*, 768–771.
- (20) Gierz, I.; Riedl, C.; Starke, U.; Ast, C. R.; Kern, K. *Nano Lett.* **2008**, *8*, 4603–4607.
- (21) Cui, Y.; Gao, J.; Jin, L.; Zhao, J.; Tan, D.; Fu, Q.; Bao, X. *Nano Res.* **2012**, *5*, 352–360.
- (22) Mao, J.; Huang, L.; Pan, Y.; Gao, M.; He, J.; Zhou, H.; Guo, H.; Tian, Y.; Zou, Q.; Zhang, L. *Appl. Phys. Lett.* **2012**, *100*, 093101.
- (23) Meng, L.; Wu, R.; Zhou, H.; Li, G.; Zhang, Y.; Li, L.; Wang, Y.; Gao, H. J. *Appl. Phys. Lett.* **2012**, *100*, 083101.
- (24) Perdew, J. P.; Zunger, A. *Phys. Rev. B: Condens. Matter Mater. Phys.* **1981**, *23*, 5048.
- (25) Kresse, G.; Hafner, J. *Phys. Rev. B: Condens. Matter Mater. Phys.* **1993**, *47*, 558.
- (26) Kresse, G.; Furthmüller, J. *Comput. Mater. Sci.* **1996**, *6*, 15–50.
- (27) Blöchl, P. E. *Phys. Rev. B: Condens. Matter Mater. Phys.* **1994**, *50*, 17953.
- (28) Henkelman, G.; Uberuaga, B. P.; Jónsson, H. *J. Chem. Phys.* **2000**, *113*, 9901–9904.
- (29) Marchini, S.; Gunther, S.; Wintterlin, J. *Phys. Rev. B: Condens. Matter Mater. Phys.* **2007**, *76*, 075429.
- (30) Pan, Y.; Zhang, H. G.; Shi, D. X.; Sun, J. T.; Du, S. X.; Liu, F.; Gao, H. J. *Adv. Mater.* **2009**, *21*, 2777–2780.
- (31) Wang, B.; Bocquet, M. L.; Marchini, S.; Gunther, S.; Wintterlin, J. *Phys. Chem. Chem. Phys.* **2008**, *10*, 3530–3534.
- (32) Cattelan, M.; Agnoli, S.; Favaro, M.; Garoli, D.; Romanato, F.; Meneghetti, M.; Barinov, A.; Dudin, P.; Granozzi, G. *Chem. Mater.* **2013**, *25*, 1490–1495.
- (33) Wang, D. W.; Li, F.; Chen, Z. G.; Lu, G. Q.; Cheng, H. M. *Chem. Mater.* **2008**, *20*, 7195–7200.
- (34) Panchakarla, L. S.; Subrahmanyam, K. S.; Saha, S. K.; Govindaraj, A.; Krishnamurthy, H. R.; Waghmare, U. V.; Rao, C. N. R. *Adv. Mater.* **2009**, *21*, 4726–4730.
- (35) Que, Y. D.; Xiao, W. D.; Fei, X. M.; Chen, H.; Huang, L.; Du, S. X.; Gao, H. J. *Appl. Phys. Lett.* **2014**, *104*, 093110.
- (36) Leenaerts, O.; Partoens, B.; Peeters, F. M. *Phys. Rev. B: Condens. Matter Mater. Phys.* **2008**, *77*, 125416.
- (37) Ren, J. D.; Guo, H. M.; Pan, J. B.; Zhang, Y. Y.; Wu, X.; Luo, H.-G.; Du, S. X.; Pantelides, S. T.; Gao, H.-J. *Nano Lett.* **2014**, *14*, 4011–4015.
- (38) Sutter, E.; Acharya, D. P.; Sadowski, J. T.; Sutter, P. *Appl. Phys. Lett.* **2009**, *94*, 133101.